Journal of Physical Sciences, Vol. 19, 2014, 129-141
ISSN: 2350-0352 (print), www.vidyasagar.ac.in/journal
Published on 26 December 2014

Intense photoluminescence Emission Behavior of Pure and Doped SnO_2 Nanoparticles Synthesized via Solvothermal Technique

K. Anandan and V. Rajendran

Department of Physics, Presidency College, Chennai 600 005, Tamilnadu, India
E-mail address: anand.nanoscience@yahoo.com; ab.nanoscience@gmail.com

Received 2 September 2014; accepted 2 December 2014

ABSTRACT

Niobium and zirconium doped tin oxide (SnO_2) nanoparticles have been successfully synthesized via the solvothermal technique. The Size, structure, morphology and composition of the as-synthesized samples were characterized by powder X-ray diffraction (XRD), Fourier transform infrared (FTIR) spectroscopy, scanning electron microscopy (SEM), transmission electron microscopy (TEM) and energy dispersive X-ray (EDX) spectroscopy. The optical properties of the samples were investigated by ultraviolet–visible (UV-vis) and photoluminescence (PL) spectroscopies. The magnetic property was studied with the vibrating sample magnetometer (VSM). Finally, the possible formation mechanism for synthesized tin oxide has also been proposed.

Keywords: Semiconductors; SnO_2 nanoparticles; Solvothermal process; Optical properties

1. Introduction

Today, one of the most rapidly developing fields of knowledge is nanotechnology. One of the parts of this broad field is nanomaterials, i.e., materials with one or more dimensions in the range of 1-100 nm (powders, layers or bulk materials). Among the other known oxide semiconductors, tin oxide (SnO_2) is a very interesting material with a wide band gap (Eg = 3.6 eV). Recently, there has been an increasing interest in the research of the wide band gap semiconductor SnO_2 nanoparticles, with a rutile type tetragonal crystalline structure [1]. Owing to its excellent optical properties, as well as outstanding chemical and physical stabilities, SnO_2 has been extensively used for photovoltaic devices [2], gas sensors [3], catalysts, solar cells [4] and flat-panel displays in the field of transparent conducting electrodes [5] and so on. For low cost and portable applications, metal oxide sensors are commonly used to monitor various toxic and inflammable gases in environmental protection, healthcare, and automobiles. The Preparation of these materials in the nanoscale range helps in getting increased surface-to-volume ratio which might affect the structural and most other physical properties. Recent research work has been devoted to the development of the synthesis of SnO_2 nanoparticles of varied sizes in a controllable manner. The doping of transition metal ions into SnO_2 systems is of great interest due to their ability in tuning the size, and structural and morphological properties [6–8]. The optoelectronic properties such as photoluminescence and optical band gap of SnO_2 can also be improved by impurity

doping, which helps in their applications in sensors and other optoelectronic devices [9, 10]. Among the different techniques, the solvothermal technique can be used to control the grain size, structure, morphology, and surface chemistry by regulating the reaction temperature, pressure, solvent nature, additives and aging time. Nano-sized particles prepared by using the solvothermal technique are expected to have a larger surface area, smaller particle size, and greater stability than those obtained by other methods such as the sol-gel method.

This paper reports the effect of Nb and Zr doping, on the structural and optical properties of SnO_2 nanoparticles, prepared by the solvothermal technique. Analyses were carried out using techniques like XRD, FTIR, SEM, TEM, EDAX, UV-visible, PL and VSM.

2. Materials and methods

2.1. Synthesis of pure and doped tin oxide nanoparticles

A closed cylindrical Teflon-lined stainless steel autoclave with 100 ml capacity was used for the synthesis. All the reagents and solvents used were of analytical grade and without any further purification. In a typical synthesis, 5 ml of $SnCl_4$ was taken with 50 ml of solvent (3:2 ratios of absolute ethanol and distilled water) in a beaker and dissolved in 1.26 g of oxalic acid. After a few minutes of vigorous stirring, the required amount of niobium pentoxide (Nb_2O_5) was added to the solution and dissolved completely. The transparent solution was poured into the autoclave and filled with absolute ethanol up to 80% of the autoclave, and maintained at 250°C for 24h. After the reaction time, the autoclave was allowed to cool down naturally and the resulting precipitates were carefully washed with distilled water and absolute ethanol repeatedly, more than 5 times for the removal of Cl^- ion, and to avoid aggregation and then dried in vacuum at 60°C for 5h. The final product was characterized by the following methods. For comparison, pure and zirconium (zirconium oxychloride: $ZrOCl_2.8H_2O$) doped SnO_2 nanoparticles were prepared with the same procedure, as described previously. The samples were named as (A) pure, (B) Nb-doped and (C) Zr-doped SnO_2 nanoparticles.

2.2. Characterization of as-synthesized nanoparticles

The particles size and structure of the samples were identified by powder X-ray powder diffraction using Seifert (JSO-DEBYFLEX 2002) diffractometer with monochromatized CuKα1 radiation (λ = 0.1541 nm). The XRD data were collected over a 2θ range from 20° to 70° at a scanning rate of 5°/min. The functional groups of the samples were observed by Fourier transform infrared spectra using a Nicolet-205 spectrometer. The morphology of the samples were collected from the scanning electron microscopic image was carried out by Hitachi S-4500 (Hitachi, Japan). The crystalline size and morphology of the samples were further confirmed by transmission electron microscopy performed on a JOEL-3010 electron microscope operated at 120 kV, accompanied by energy dispersive X-ray analysis attachment for the compositional analysis. Ultraviolet–visible absorption spectra were obtained from a Varian Cary 5E spectrophotometer in the range of 200–800 nm. The room temperature photoluminescence measurements were carried out on a Fluoromax-4 spectrofluorometer with a Xe lamp as the excitation light source. The magnetic measurement was carried out in a vibrating sample magnetometer (VSM; BHV-55, Riken, Japan) at room temperature.

3. Results and discussion

The size and structural properties of the as-synthesized samples were characterized by XRD and FTIR studies. Fig. 1 (a-c) shows the XRD pattern of samples A, B and C, respectively. Characteristic peaks with intensities corresponding to the (110), (101), (200), (111), (211), (220), (002), (310) (112) and (301) planes were observed, which indicate that the sample is of high purity, with a rutile tetragonal structure (JCPDS card No.41-1445). It is clear that there are no extra peaks due to niobium and zirconium metal oxides, implying that the transition metal ions get substituted at the Sn site without changing the rutile tetragonal structure. The crystallinity of the samples was significantly affected by the Zr and Nb ions in the SnO_2. It can be found that the diffraction peak of the doped SnO_2 samples was wider than that of the pure SnO_2 sample. The pattern indicates that the size of the doped SnO_2 nanoparticles is smaller than that of the pure SnO_2 nanoparticles.

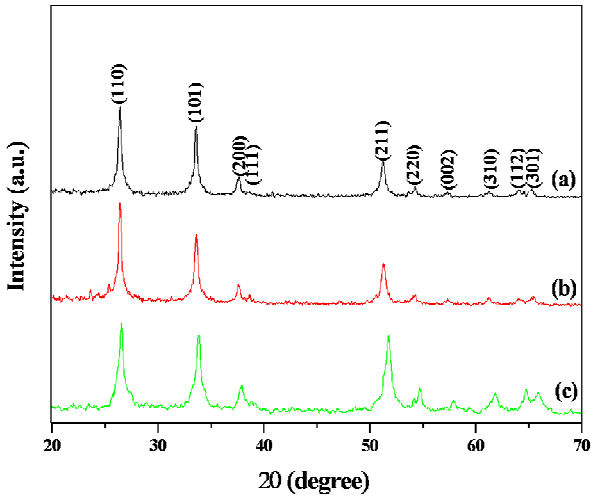

Figure 1. Powder XRD patterns of (a) pure, (b) Nb-doped and (c) Zr-doped SnO_2 nanoparticles.

Furthermore, the average crystallite size was calculated by using the Debye-Scherrer's formula;

$$D = 0.9\lambda / \beta\cos\theta \quad (1)$$

where D, λ, β, and θ are the particle size, CuKα1 radiation (0.1541 nm), full width at half maximum (FWHM) of the diffraction peak and Bragg angle, respectively. The calculated average particles sizes were 24.2, 20.4 and 16.6 nm for pure SnO_2, Nb-SnO_2 and Zr-SnO_2 nanoparticles, respectively. Besides, from the values it is interesting to note, that the grain

size decreases considerably, when the transition metal ions are inserted into the SnO_2 matrix.

The FTIR spectra were recorded in the solid phase using the KBr pellet technique in the region of 4000–400 cm^{-1} as shown in Fig. 2. The broad and narrow bands observed at ~3475 and 1622 cm^{-1} indicate the presence of hydroxyl groups [11], which is probably due to the fact that the spectrum was not recorded in situ, and some readsorption of water from the ambient atmosphere has occurred. The bands appearing at ~949 and 1120 cm^{-1} are related to the vibration of tin-hydroxyl (Sn–OH) bond [12]. The broad band at ~ 850 – 447 cm^{-1} is associated with the O–Sn–O bridge functional groups of SnO_2, which confirms the presence of SnO_2 in the crystalline phase [12]. This is in good agreement with the results of the XRD analysis.

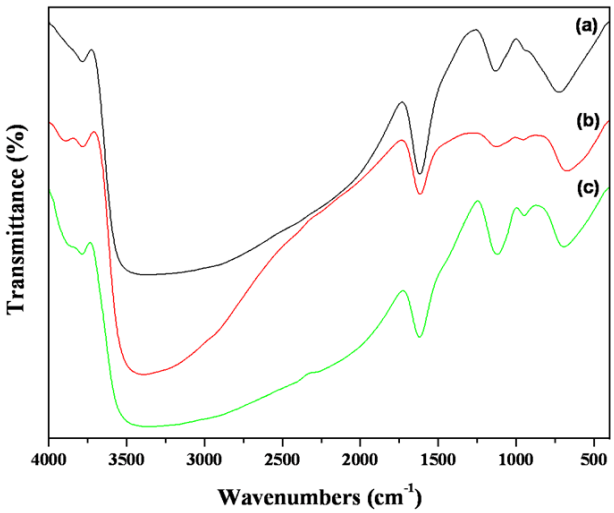

Figure 2. FTIR spectra of (a) pure, (b) Nb-doped and (c) Zr-doped SnO_2 nanoparticles.

Fig. 3 (a-c) shows the SEM images of samples A, B and C, respectively. All the samples show spherical shaped SnO_2 nanoparticles, while pure and Nb-SnO_2 show the aggregated particles. The Zr-SnO_2 nanoparticles were improved, as only a few agglomerates appeared, and the dispersion was better than that of the pure SnO_2 and Nb-SnO_2 samples. However, on the whole, it was clear that doping can inhibit the excess aggregation of SnO_2 nanoparticles. This indicates that the Nb and Zr doping into SnO_2 can change the surface character of the primary nanoparticles, which was deduced to be from the effects of the diffusion of Nb^{5+} and Zr^{4+} into the SnO_2 lattice, and the formation of a Nb–O–Sn and Zr–O–Sn bond on the surface of the doped samples.

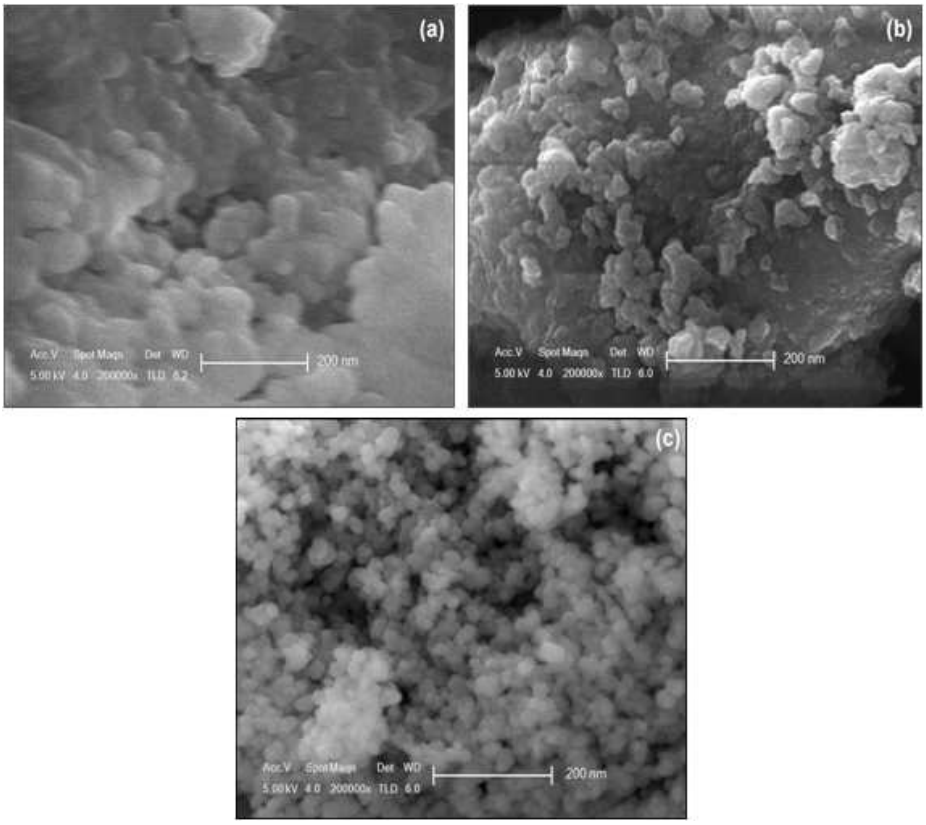

Figure 3. Spherical shaped SEM images of (a) pure, (b) Nb-doped and (c) Zr-doped SnO_2 nanoparticles.

Fig. 4 (a-c) shows the TEM images of samples A, B and C, respectively. For the TEM imaging, the sample powders were dispersed in methanol by using ultrasonic radiation for 10 min and a drop of the suspension was placed onto the carbon-coated grids. The images reveal that most of the particles have been formed as fine spheres in the all samples, while in the pure SnO_2 nanoparticles some are elongated. Well-dispersed particles were observed for the Nb and Zr doped samples. However, a slight aggregation of particles has been observed in the pure samples. The corresponding selected area electron diffraction (SAED) patterns (inserted) show that the polycrystalline rings are indexed to the rutile tetragonal structure of SnO_2, which are in good agreement with the XRD results.

From the data obtained by the TEM images, the mean size and histograms of the particles can be determined and drawn. Fig. 5 (a-c) shows the particle size distribution of the samples A, B and C, respectively. It can be seen that the particle sizes possess a small and narrow size distribution in the range from 4 to 36 nm, and the mean diameters are about 24, 20 and 16 nm for the samples A, B and C, respectively. It is noticed that the mean

particle size determined by the TEM study is in good agreement with the average crystallite size, calculated by Scherrer's formula from the XRD patterns. According to the TEM images, it could be concluded that this preparation method was successful to obtain SnO_2 nanoparticles with well-dispersed and smaller spherical particles.

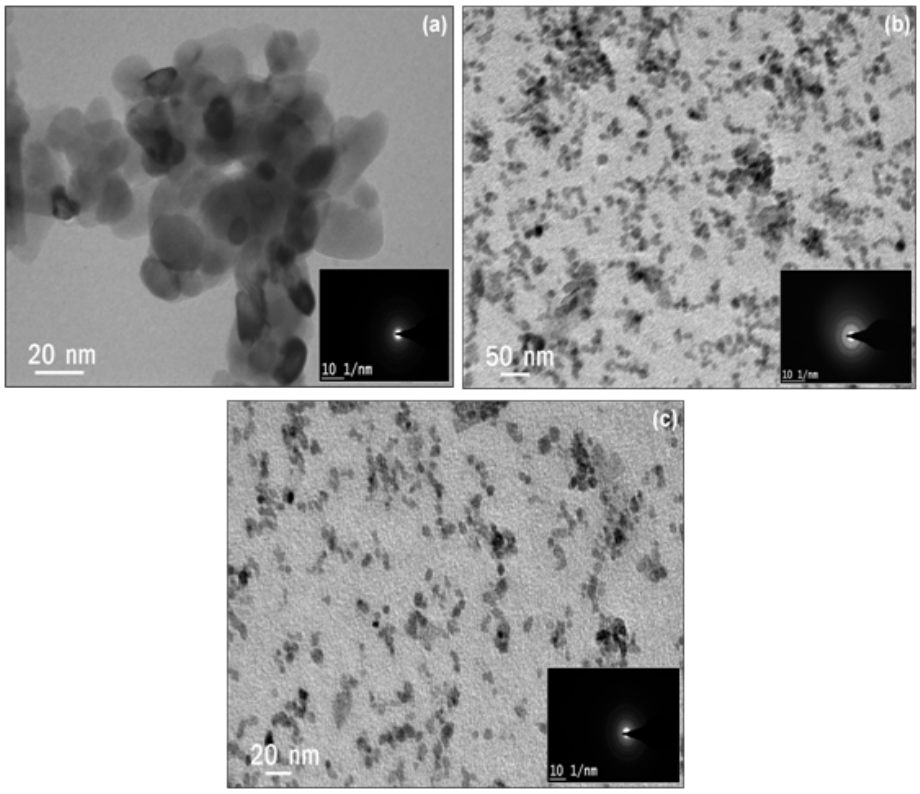

Figure 4. TEM images of (a) pure, (b) Nb-doped and (c) Zr-doped SnO_2 nanoparticles.

The EDX spectrum is used to confirm the composition of the samples. The EDX spectrum has been taken directly from the combined TEM instrument. Fig. 6 (a and b) depicts the EDX spectra of the pure SnO_2 and Zr-SnO_2 nanoparticles. The image showed the presence of Sn and O as the only elementary species in the pure SnO_2 sample (Fig. 6a), and with the addition of Zr as the doped elementary in the Zr-doped SnO_2 sample (Fig. 6b), which clearly shows the existence of Zr ion in the sample, and confirms the successful doping of Zr in SnO_2. The presence of Cu in both the images is due to the copper grid. The quantitative analysis reveals the atomic ratio of Sn, O and Zr as 33.30:66.70 and 19.35:79.53:1.12 which is consistent with the atomic ratio of the pure SnO_2 and Zr-SnO_2 nanoparticles, respectively.

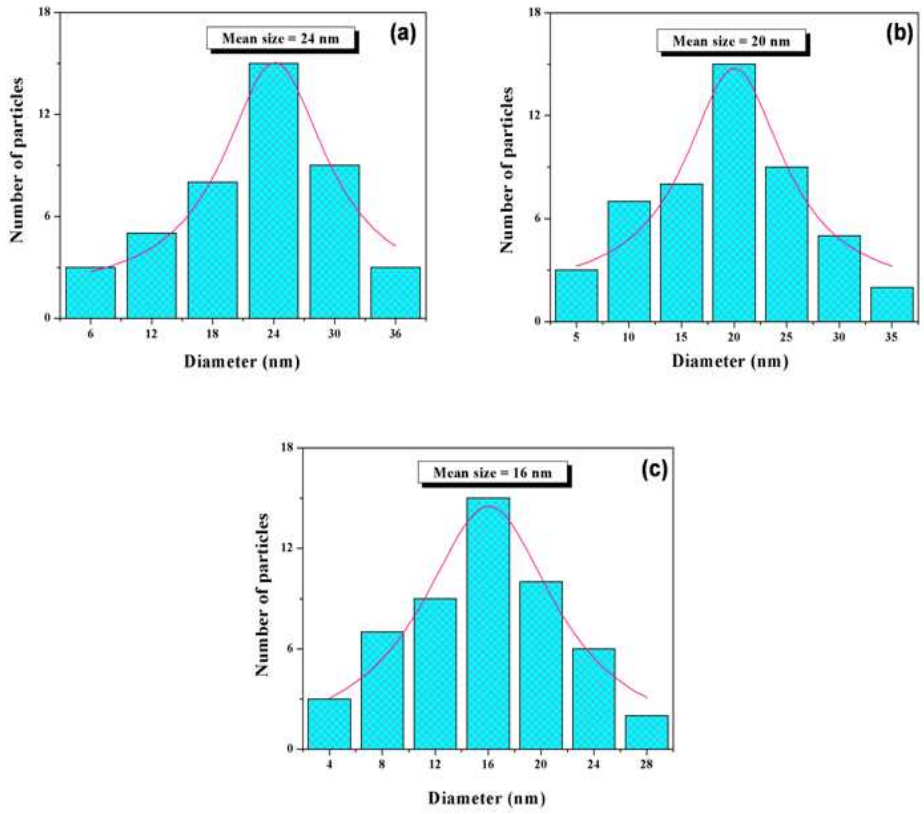

Figure 5. Particles size distribution of TEM images: (a) pure, (b) Nb-doped and (c) Zr-doped SnO_2 nanoparticles.

Absorption and fluorescence spectroscopies are powerful non-destructive techniques to explore the optical properties of semiconducting nanoparticles. The optical absorption spectra of the pure and doped SnO_2 nanoparticles are shown in Fig. 7. The absorbance is expected to depend on several factors, such as the band gap, oxygen deficiency surface roughness and impurity centers. The UV-visible absorption spectra were recorded in the incident photon wavelength of 200–800 nm. The absorption edge of pure SnO_2, Nb-SnO_2 and Zr-SnO_2 nanoparticles varies. The band gap energy is an important electronic parameter to characterize semiconductor nanomaterials. The direct band gaps of the nanoparticles were determined from the well known Tauc relation [13] given by:

$$\alpha h\nu = A(h\nu - E_g)^n \quad (2)$$

where α, h, n, A and E_g are the absorption coefficient (α=2.303 A/t, A is the absorbance, t is the thickness of the cuvette) Planck's constant, light frequency, frequency-independent

constant and band gap energy, respectively, and n=1/2 for the direct band gap semiconductor.

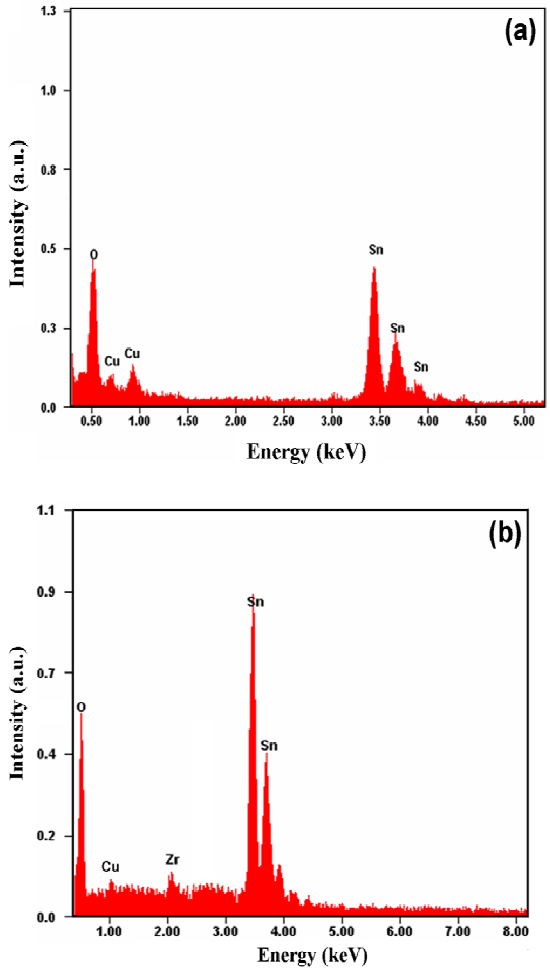

Figure 6. EDX patterns of (a) pure and (b) Zr-doped SnO_2 nanoparticles.

The optical band gap energy (E_g) of the samples was estimated from the Tauc curves by plotting $(\alpha h\nu)^2$ versus the photon energy ($h\nu$). An extrapolation of the linear region of a plot of $(\alpha h\nu)^2$ versus $h\nu$ gives the value of the optical band gap E_g (inset of Fig. 7). By the incorporation of the transition metal ions into the SnO_2 nanoparticles, blue shifts are seen in the absorption spectra [14]. This observation suggests that impurity levels are introduced between the intrinsic bands of the SnO_2 nanoparticles, which subsequently generate new band gaps. The measured band gap was found to be 4.06, 3.99 and 3.92 eV for Zr-SnO_2, Nb-SnO_2 and pure SnO_2 nanoparticles, respectively, which is higher than the reported value of the bulk SnO_2, i.e., 3.6 eV [15]. This implies that when the average particle sizes decrease the width of the band gap increases. The increasing trends of the

band gap energy upon the decreasing particle size are well presented for the pure and doped SnO_2 nanoparticles and are shown in Fig.8.

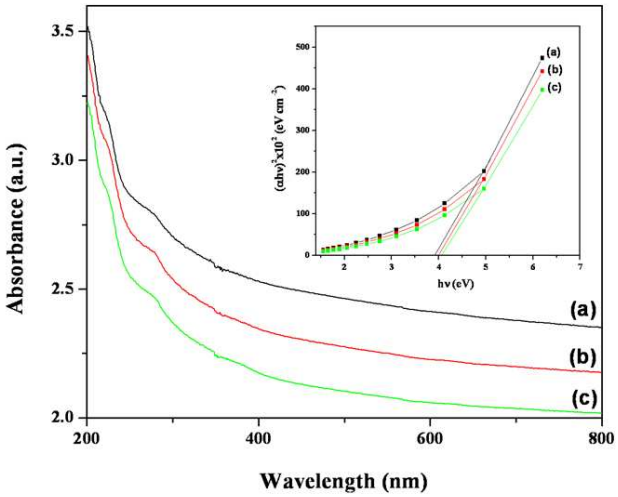

Figure 7. UV-vis absorption spectra of (a) pure, (b) Nb-doped and (c) Zr-doped SnO_2 nanoparticles: the inset of $(\alpha h\nu)^2$ versus $h\nu$ curve of the samples.

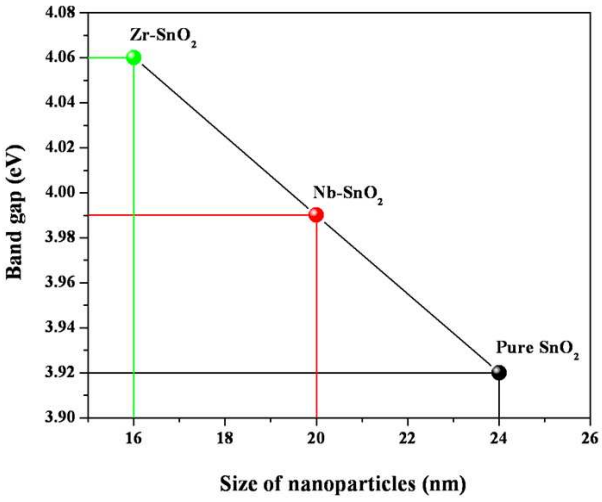

Figure 8. Size of nanoparticles versus band gap energy of synthesized samples.

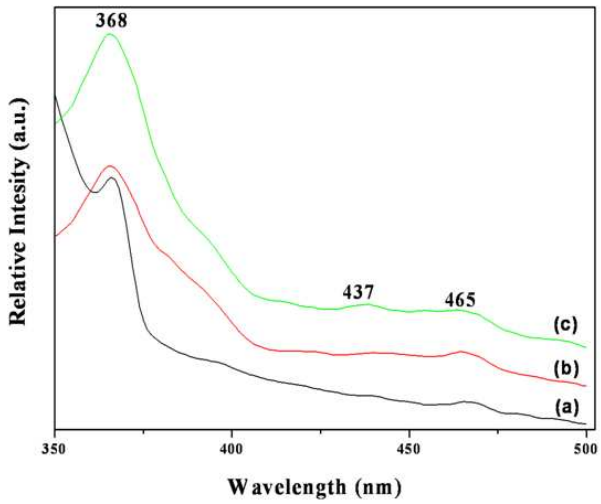

Figure 9. Room temperature photoluminescence spectra of (a) pure, (b) Nb-doped and (c) Zr-doped SnO_2 nanoparticles.

Photoluminescence characterization is another effective method to study the intrinsic nature of SnO_2, such as oxygen vacancies and energy bands. Fig. 9 shows the room temperature photoluminescence spectra of pure SnO_2, Nb-SnO_2 and Zr-SnO_2 nanoparticles with an excitation wavelength of 325 nm. There are three emission peaks centered in all the samples at wavelengths of 368, 437 and 465 nm, respectively. In the UV emission region, the 368 nm peak with the corresponding energy of 3.36 eV is called as the near band edge emission (NBE), which is likely to be associated with a band-to-band recombination process, possibly involving localized or free excitons (ΔE_{NBE} = 3.36 eV) [16,17]. The other two peaks centered in the blue emission region, 437 and 465 nm, with the corresponding energy of 2.83 and 2.67 eV, are obviously lower than the deduced band gap, and are attributed to the presence of oxygen vacancies on the surface. From PL spectra, it can be seen that the Nb and Zr doped samples show broad and prominent emission peaks than the pure SnO_2 samples. In the pure SnO_2 host, the emission is attributed to electron transmission, mediated by defect levels in the band gap, such as oxygen vacancies, tin interstitials and so forth. Probably, after incorporating the Nb and Zr ions into the SnO_2 host matrix, the defect still plays a dominant role, with respect to the luminescence processes. These results indicate the good crystalline quality of nanoparticles obtained in the doped samples. Generally, oxygen vacancies are known to be the most common defects in semiconductor nanocrystals and usually act as radiative centers in the luminescence processes. In SnO_2, the oxygen vacancies are present in three different charge states: V_o^o, V_o^+ and V_o^{++}, in which V_o^o is a very shallow donor [18]. The recombination of the surface trapped hole with an electron in a deep trap (V_o^+) to form a V_o^{++} center, gives rise to visible emission when a conduction band electron recombines with the V_o^{++} center. Hence, the observed photoluminescence emission spectra can be attributed to an effect of crystallite size reduction and defect of oxygen vacancies in the

nanoparticles, as a result of Nb and Zr doping in SnO_2 nanoparticles. It is known that in a bulk system, the effect of the oxygen vacancies is not important, as the density of oxygen vacancies is very low. However, when the grain dimensions are reduced to nanometric scale the translational symmetry breaking and the low coordination at the surface lead to the occurrence of oxygen vacancies, whose density strongly increases as the particle size decreases. Those oxygen vacancies, mainly located on the particle surface, are thought to play a key role in the ferromagnetism observed in nanosized SnO_2 [19]. It is well known that normally after several months of synthesis, samples tend to lose oxygen. As for our SnO_2 powders, after a few months, when we measured the samples again, we found an increase in the magnetic moment. It is likely that those two features are combined, when supposing that magnetism is due to oxygen vacancies: since there are more oxygen vacancies in the sample, the magnetic moment could be observed.

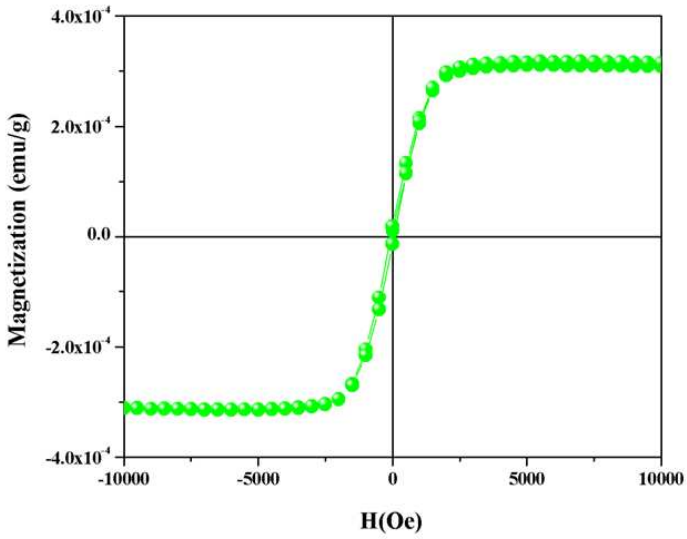

Figure 10. Magnetic moment (m) vs. magnetic field (H) obtained at 300 K for Zr-SnO_2 nanoparticles.

Fig. 10 shows the dependence of the magnetic moment (m) of the Zr-SnO_2 nanoparticles as a function of the magnetic field (H) obtained at 300 K. The s-shaped curve observed in the central part for the sample data suggests that a magnetic order is happening. The image clearly shows that the ferromagnetic behavior of the synthesized SnO_2 nanoparticles with the size of 16 nm. As the particle size increases, the ferromagnetic signal is expected to reduce, since the vacancy population decreases. This is thought to be the origin of the ferromagnetism observed in the 16 nm SnO_2 nanoparticles in this work, and it must be the reason why a weaker ferromagnetic signal is observed in the 20 nm SnO_2 nanoparticles in [20].

During the solvothermal treatment, it is likely that the crystal is grown via the "dissolution – recrystallization" process, which can be divided into three stages; at the start of the reaction, with the increase in temperature, the SnO_2 amorphous precipitate is gradually dissolved in the aqueous ethanol solution**;** then the recrystallization of SnO_2 takes place when the concentration of SnO_2 in the solution reaches super saturation; the last stage is crystal growth. Thus, the SnO_2 concentrations and the chemical potential increased and the addition of dopants, resulted in the formation of different sized particles, which exhibits good structural and optical properties due to the dopants effects.

4. Conclusion

In conclusion, the successful synthesis of high purity, pure and transition metal (Nb and Zr) ions doped tin oxide (SnO_2) nanoparticles has been achieved via the solvothermal technique. The crystalline size was calculated from the Scherer's formula, which suggested the formation of nanoparticles, and this was further confirmed by the TEM images. The morphologies of the samples were observed from the SEM images, which show that most of the particles were spherical in shape. The EDX spectra show that the Zr ion is successfully incorporated into the SnO_2 nanoparticles. Optical studies have been carried out, using optical absorbance and fluorescence spectroscopies. The band gap was measured for the pure and doped samples, by using the Tauc relation of 3.92 – 4.06 eV. This can be attributed to the quantum confinement effect of the SnO_2 nanoparticles. The increasing trends of the band gap energy upon the decreasing particle size are well presented for the pure and doped samples. The fluorescence spectra show a broad visible emission peak, which may be due to the surface defect levels. The intensity of visible emission increases as the dopants are introduced into SnO_2 nanoparticles, which indicates the good crystalline quality of nanoparticles obtained in the synthesized samples. Thus, the niobium and zirconium doping can be used as a method to control the band gap and visible luminescence of the SnO_2 nanoparticles. The synthesized Zr-SnO_2 nanoparticles show the ferromagnetic behavior in the vibrating magnetometer sample measurement strongly. Furthermore, the method has the important advantage of being simple and fast and can be extended to the synthesis of many other oxide nanoparticles. This work would be meaningful if it provides a methodology to synthesize ultra-fine nanomaterials for the use of versatile applications.

REFERENCES

1. K.K. Khun, A. Mahajan and R.K. Bedi, Nanostructured Sb doped SnO_2 thick films for room temperature NH_3 sensing, *Chemical Physics Letters,* 492 (2010) 119–122.
2. H.L. Hartnagel, A.L. Dewar, A.K. Jain and C. Jagadish, *IOP, Bristol,* (1995).
3. Z.R. Dai, Z.W. Pan and Z.L. ang, Novel Nanostructures of Functional Oxides Synthesized by Thermal Evaporation, *Advanced Functional Materials,* 13 (2003) 9–25.
4. D.F. Zhang, L.D. Sun, J.L. Yin and C.H. Yan, Low-temperature fabrication of highly crystalline SnO_2 nanorods, *Advanced Materials,* 15 (2003) 1022–1025.
5. B.G. Lewis and D.C. Paine, Applications and processing of transparent conducting oxides, *MRS Bulletin,* 25 (2000) 22–27.

6. O. Wurzinger and G. Reinhardt, CO-Sensing Properties of Doped SnO_2 Sensors in H_2-Rich Gases, *Sensors Actuators B*: *Chemical*, 103 (2004) 104–110.
7. H. Yang, X. Song, X. Zhang, W. Ao and G. Qiu, Synthesis of vanadium-doped SnO_2 nanoparticles by chemical co-precipitation method, *Materials Letters*, 57 (2003) 3124–3127.
8. A. Maciel, P. Lisboa-Filho, E. Leite, C. Paiva-Santos, W. Schreiner, Y. Maniette and E. Longo, Microstructural and morphological analysis of pure and Ce-doped tin dioxide nanoparticles, *Journal of the European Ceramic Society*, 23 (2003) 707–713.
9. P. Singh, A.K. Chawla, D. Kaur and R. Chandra, Effect of oxygen partial pressure on the structural and optical properties of sputter deposited ZnO nanocrystalline thin films, *Materials Letters*, 61 (2007) 2050–2053.
10. Y.J. Ma, F. Zhou, L. Lu and Z. Zhang, Low-temperature transport properties of individual SnO_2 nanowires, *Solid State Communications*, 130 (2004) 313–316.
11. K. Anandan and V. Rajendran, A Low-temperature Synthesis and Characterization of Tetragonal-ZrO_2 Nanoparticles via Simple Hydrothermal Process, *Journal of Physical Sciences*, 17 (2013) 179–184.
12. A. Azam, A.S. Ahmed, S.S. Habib and A.H. Naqvi, Effect of Mn doping on the structural and optical properties of SnO_2 nanoparticles, *Journal of Alloys Compounds*, 523 (2012) 83–87.
13. J. Tauc , R. Grigorovici and A. Vancu, Optical Properties and Electronic Structure of Amorphous Germanium, *Physica Status Solidi B*, 15 (2006) 627–637.
14. T. Takagahara and K. Takeda, Theory of the quantum confinement effect on excitons in quantum dots of indirect-gap materials, *Physical Review B*, 46 (1992) 15578–15581.
15. K. Anandan and V. Rajendran, Rose-like SnO_2 Nanostructures Synthesized via Facile Solvothermal Technique and their Optical Properties, *Journal of Physical Sciences*, 14 (2010) 227–234.
16. S.S. Pan, C. Ye, X.M. Teng, L. Li and G.H. Li, Localized exciton luminescence in nitrogen-incorporated SnO_2 thin films, *Applied Physics Letters*, 89 (2006) 251911.
17. M.M. Rashad, E.M. Elsayed, M.M. Moharam, R.M. Abou-Shahba and A.E. Saba, Structure and magnetic properties of $Ni_xZn_{1-x}Fe_2O_4$ nanoparticles prepared through co-precipitation method, *Journal of Alloys Compounds*, 485 (2009) 759–767.
18. K. Vanheusden, W.L. Warren, C.H. Seager, D.R. Tallant, J.A. Voigt, B.E. Gnade, Mechanisms behind green photoluminescence in ZnO phosphor powders, *Journal of Applied Physics*, 79 (1996) 7983–7990.
19. S.A. Ahmed, Room-temperature ferromagnetism in pure and Mn doped SnO_2 powders, *Solid State Communications*, 150 (2010) 2190–2193.
20. A. Punnoose, K.M. Reddy, J. Hays and A. Thurber, Magnetic gas sensing using a dilute magnetic semiconductor, *Applied Physics Letters*, 89 (2006) 112509.